ACS APPLIED MATERIALS & INTERFACES

Research Article

www.acsami.org

High Efficiency Air-Processed Dithienogermole-Based Polymer Solar Cells

Iordania Constantinou,[†] Tzung-Han Lai,[†] Dewei Zhao,[†,§] Erik D. Klump,[†] James J. Deininger,[‡] Chi Kin Lo,[‡] John R. Reynolds,[‡] and Franky So*[,†]

[†]Department of Materials Science and Engineering, University of Florida, Gainesville, Florida 32611, United States

[‡]School of Chemistry and Biochemistry, School of Materials Science and Engineering, Center for Organic Photonics and Electronics, Georgia Institute of Technology, Atlanta, Georgia 30332, United States

ABSTRACT: The effect of air processing, with air exposure varying from minutes to hours prior to encapsulation, on photovoltaic device performance has been studied through a series of electrical characterizations and optical simulations for a donor/acceptor polymer-based organic solar cell based on poly(dithienogermole-*alt*-thienopyrrolodione) p(DTG-TPD)/$PC_{71}BM$ blends. A ∼10% degradation in power conversion efficiency was observed due to air processing with 10 min exposure time, with AM1.5 power conversion efficiencies (PCEs) decreasing from 8.5 ± 0.25% for devices processed in inert nitrogen atmosphere to 7.7 ± 0.18% for devices processed in ambient air. After 3 h air exposure, the PCE leveled off at 7.04 ± 0.1%. This decrease is attributed partially to interface issues caused by exposure of the electrode materials to oxygen and water and partially to a degradation of the hole transport in the active layer.

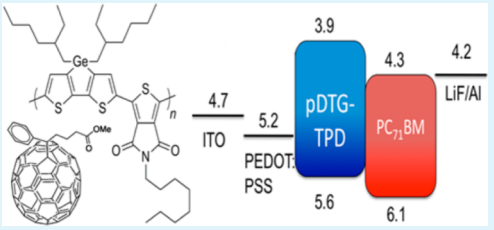

KEYWORDS: *solar cells, organic photovoltaics, air processing, conjugated polymers, dithienogermole, fullerenes, charge mobility*

1. INTRODUCTION

Polymer solar cells (PSCs) have attracted an increased interest over the past decade since they potentially offer a less expensive and more sustainable alternative for solar energy harvesting.[1] At the same time they offer additional features such as ambient temperature solution processability, mechanical flexibility, and light weight.[2] Laboratory scale power conversion efficiencies (PCEs) for bulk heterojunction (BHJ) PSCs based on conjugated polymers and fullerene derivatives have been steadily increasing and are currently approaching 10%,[3,4] while π-conjugated molecule:fullerene cells have also reached 10%[5] and polymer:polymer cells have reached 6%.[6] In order for PSCs, and organic solar cells in general, to reach their full potential, device processing must become compatible with high volume manufacturing processes with interfacial layers, active layers, and electrodes all deposited under air ambient conditions.

Since polymer solar cells can be processed from solution, they present versatility in their production methods. The most attractive advantage for PSCs is the possibility for high-throughput production on flexible substrates using deposition techniques compatible with roll-to-roll (R2R) processing such as slot-die coating, ink jet printing, and spray coating.[7] Compared to devices fabricated on the laboratory scale (ca. 0.1−1 cm^2 in area), PSCs fabricated by R2R processing usually have lower PCEs.[8] The lower efficiency is mainly due to the difference in device structures and deposition processes required for R2R processing which include large-area devices, thick active layers, and air ambient processing.[9,10] Despite the fact that air ambient processing is necessary for high-volume manufacturing, most laboratory devices reported are still fabricated in inert environments.[11] This is mainly due to the fact that exposure to oxygen and water has been shown to damage the organic semiconductors used in the devices, hence degrading performance.[12,13] For the eventual commercialization of PSCs, it will be highly advantageous to use all ambient processing. It is therefore important to study the effects of ambient processing on high-performance PSCs in order to understand the associated degradation mechanisms.

To date, most studies on air-processed solar cells found in the literature are focused on devices based on blends of poly(3-hexylthiophene) (P3HT) and [6,6]-phenyl-C61-butyric acid methyl ester ($PC_{60}BM$).[14] Recently, Wu et al. studied the effect of air processing on P3HT:$PC_{60}BM$ device performance. They found that P3HT:$PC_{60}BM$ devices processed in ambient air conditions can exhibit reversible degradation upon annealing, therefore exhibiting good air processability.[15] This is in agreement with other reports on the formation of a reversible charge transfer complex in P3HT due to oxygen.[16,17] While P3HT:$PC_{60}BM$ has served as the standard upon which the field was built, this material system has become less interesting due to the relatively low PCEs (∼4%) when compared to most newly developed high-performance polymers. Donor−acceptor polymer:$PC_{71}BM$ blends are now better candidates for air-processing studies since they exhibit PCEs in the range of 8−10%. Until now there have been very few reports on air-

Received: December 11, 2014
Accepted: February 10, 2015
Published: February 10, 2015

ACS Publications © 2015 American Chemical Society

DOI: 10.1021/am5087566
ACS Appl. Mater. Interfaces 2015, 7, 4826−4832

processed devices based on high-efficiency low-bandgap polymers.[18−20] While the study of air-processed devices is important for commercialization, preliminary results on highly efficient polymers such as PTB7 show significant degradation upon exposure to oxygen.[21−23]

Previously, we reported on BHJ PSCs based on poly(dithienogermole-*alt*-thienopyrrolodione) p(DTG-TPD)/$PC_{71}BM$ blends with a power conversion efficiency up to 8%.[24] We have also demonstrated that high efficiencies can be achieved with a p(DTG-TPD)/$PC_{71}BM$ active layer thickness >200 nm, a thickness that is compatible with R2R processing.[25] In this report, we studied the effect of air processing on the properties of these donor/acceptor materials and the resulting device performance. Our results show that air processing and exposure for a period of time up to 10 min leads to less than 10% degradation in power conversion efficiency, with the PCE decreasing from 8.5 ± 0.25% for devices made in nitrogen atmosphere to 7.7 ± 0.18% for the devices made in ambient air. To the best of our knowledge, this is the highest efficiency reported for devices processed in air.

2. EXPERIMENTAL SECTION

2.1. Device Fabrication. The devices used in this study have a conventional architecture with the following structure: indium tin oxide(ITO)/poly(3,4-ethylenedioxythiophene):poly(styrenesulfonate)(PEDOT:PSS)/p(DTG-TPD):$PC_{71}BM$/lithium fluoride (LiF)/aluminum (Al), where PEDOT:PSS was used as the hole extraction layer and LiF/Al was used as the cathode. ITO-coated glass substrates were UV ozone treated for 15 min between solvent cleaning and spin-casting of the hole transport layer. PEDOT:PSS PVP AL 4083 (Heraeus Precious Metals GmbH & Co. KG) was spin-coated on top of the ITO-coated glass substrates in ambient air conditions and annealed at 140 °C for 20 min. The average relative humidity in the laboratory during deposition was approximately 40% ± 5%. Coated with PEDOT:PSS, half of the substrates were then transferred into a glovebox filled with N_2, where the active layer was spin-coated from solution in CB:DIO (5 vol %). P(DTG-TPD) was synthesized and purified as previously reported.[26] The rest of the substrates were kept in ambient air conditions, and the active layer was spin-coated on top of PEDOT:PSS from the same solution. All substrates were then transferred to a thermal evaporator where 1 nm of LiF and 100 nm of Al were deposited on top of the active layer.

2.2. Device Characterization. Current density−voltage (J−V) characteristics were measured using a Keithley 4200 semiconductor parameter analyzer system with a Newport Thermal Oriel 94021 1000 W solar simulator, using the AM1.5 G solar spectrum at 100 mW/cm^2 incident power. Hole-only devices with a structure ITO/molybdenum oxide (MoOx)(8 nm)/active layer(90 nm)/MoOx(8 nm)/silver (Ag)(100 nm) were used for hole mobility measurements, and electron-only devices with a structure of ITO/zinc oxide (ZnO)(40 nm)/active layer(90 nm)/LiF(1 nm)/Al(100 nm) were used for electron mobilities measurements. External quantum efficiency (EQE) measurements were conducted using an in-house setup consisting of a xenon dc arc lamp, an ORIEL 74125 monochromator, a Keithley 428 current amplifier, an SR 540 chopper system, and an SR830 DSP lock-in amplifier from SRS. To measure total absorption efficiencies, (TAE) samples were tilted at 7° angle relative to beam normal in order to allow space for the detector without blocking the incident beam. The same lock-in setup was used for both EQE and TAE measurements. All thicknesses of the active layers were determined using a Dektak surface profiler.

3. RESULTS AND DISCUSSION

The objective of this work was the comparison between devices with active layers processed in air and nitrogen and the study of air ambient on the device parameters. Throughout this report, the active layers processed in nitrogen and the active layers processed in ambient air conditions are denoted by "N_2" and "Air" respectively.

In our main set of experiments, the active layers for the Air devices were exposed to air for about 10 min prior to cathode deposition. To further demonstrate the air processability of these devices, we intentionally exposed the polymer films to air for up to 3 h before cathode deposition, which resulted in a further 8% reduction in PCE to 7.04%. In order to explain the difference in device performance due to air exposure, we studied the effects of ambient processing on device parameters through electrical and optical characterizations with the aid of optical simulations.

Figure 1a shows the J−V characteristics for a reference device processed in nitrogen and an Air device exposed to ambient air conditions for 10 min during processing. The corresponding performance parameters are summarized in Table 1. It is interesting to note that processing the devices in air did not significantly affect the different device parameters. Air-processed devices showed a less than 10% decrease in short-circuit current (J_{sc}) from 15.9 to 14.6 mA/cm^2, no change in open-circuit voltage (V_{oc}) of 0.85 V, and no statistical change in fill factor (FF), resulting in a decrease in PCE close to 10%. Thus, this reduction in PCE can be attributed to the decrease in short-circuit current density (J_{sc}) alone. A similar reduction in current was also observed by Nam et al. during the investigation of the effects of air processing on the performance of P3HT:$PC_{60}BM$ BHJ solar cells. A 15% reduction in PCE due to air exposure was observed which was almost exclusively due to a reduction in J_{sc}.[27]

The decrease in J_{sc} due to air exposure might be attributed to degradation of either the optical absorption or the transport properties of the active layer. Figure 1b shows the ultraviolet−visible (UV−vis) absorption spectra of both the N_2 and Air processed active layers coated on PEDOT:PSS. As shown in Figure 1b, the absorption spectra for both films are identical, indicating that the optical properties, as well as the active layer thickness, do not change due to air exposure. Further, based on our film thickness measurements, no difference was observed in thickness due to air processing as the active layer thicknesses were determined to be 90 ± 3 nm for both devices.

In addition to absorption, EQE measurements were performed in order to determine the spectral response difference for these devices. The EQE data are shown in Figure 1c. Interestingly, the EQE spectra exhibit obvious differences in the wavelength range between 400 and 570 nm. In the 400−570 nm wavelength range, the Air device showed a slightly lower EQE than the N_2 device, which is consistent with the slight decrease in J_{sc}. However, in the longer wavelength range between 570 and 800 nm, the two EQE curves are identical.

In order to understand the origin of the decrease in EQE, the TAEs for the devices were measured, and the data are shown in Figure 2a. TAE refers to the optical absorption of the device measured in reflection, which takes into account the effects of optical interference between the incident light and light reflected off the back electrode. Light enters the device through the transparent electrode and travels through each layer to the back aluminum electrode where it is reflected. It is assumed that the reflected light from the back aluminum electrode then travels back through to the front of the solar cell, where it enters an integrating sphere and is collected by a silicon photodetector.[28]

DOI: 10.1021/am5087566
ACS Appl. Mater. Interfaces 2015, 7, 4826−4832

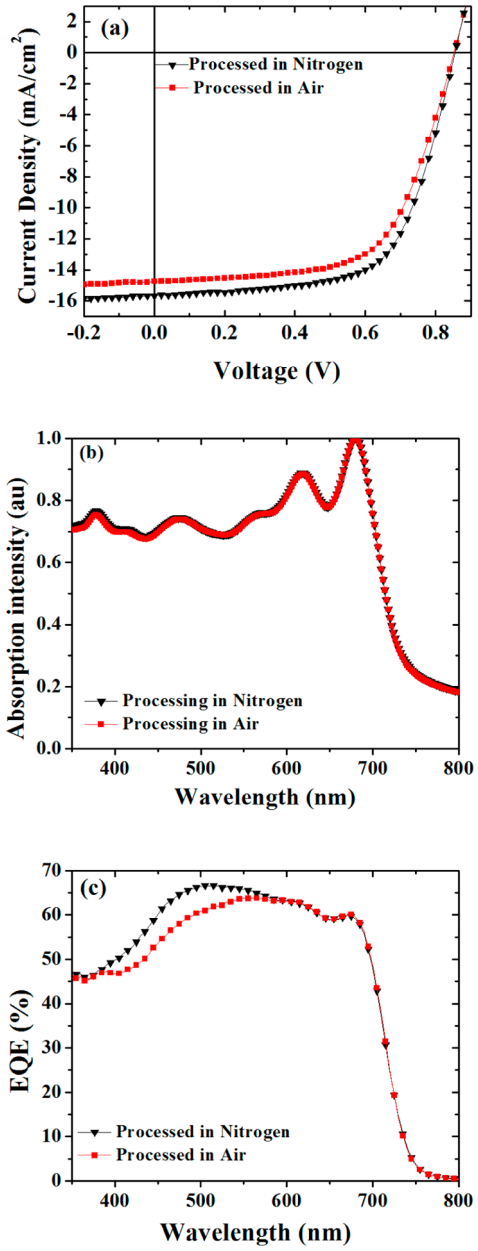

Figure 1. (a) $J-V$ curves of the solar cells made in nitrogen (black) and air (red). (b) UV−vis absorption spectra for films of polymer/fullerene blends in nitrogen and air. (c) EQE spectra of devices made in nitrogen and air.

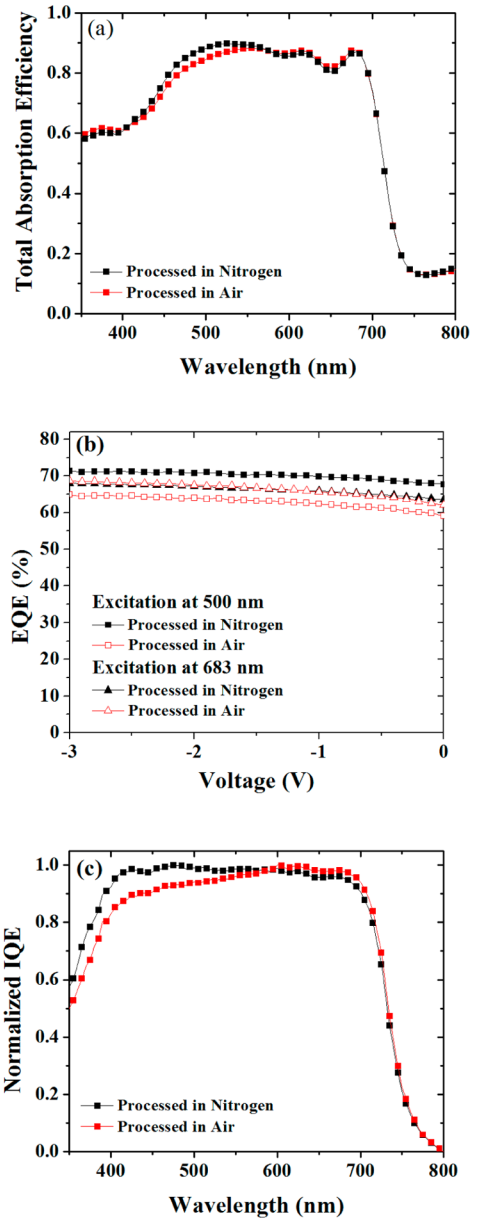

Figure 2. (a) Total absorption efficiency (TAE) in reflection for devices made in nitrogen (black) and devices made in air (red). (b) EQE as a function of reverse bias two constant excitation wavelengths, 500 and 683 nm. (c) Normalized IQE for devices made in nitrogen and devices made in air.

As expected, for wavelengths between 400 and 570 nm, the TAE for the Air device is slightly lower than that of the N_2 device, but the difference is not as pronounced as that in EQE. Since the film absorption spectra for both the N_2 and Air devices measured in transmission were the same, this difference in TAE is not attributed to a change in the active layer. Instead, it is attributed to changes in one of the interlayers that provide the electrode contacts. In order to verify our assumption that the difference in TAE is due to changes in one of the interlayers, the series resistance (R_s) for both devices was determined from $J-V$ measurements performed in the dark. An

Table 1. Summary of Average Device Characteristics for the PSCs Fabricated in This Study

atmosphere/exposure time	J_{sc} (mA/cm^2)	V_{oc} (V)	FF (%)	PCE (%)
nitrogen	15.9 (±0.17)	0.855 (±0.01)	63 (±1.7)	8.5 (±0.25)
air/10 min	14.6 (±0.3)	0.85 (±0.015)	62 (±1.4)	7.7 (±0.18)
air/1 h	13.22 (±0.13)	0.86 (±0.01)	63.5 (±0.5)	7.2 (±0.21)
air/2 h	13.0 (±0.23)	0.85 (±0.00)	64 (±0.5)	7.1 (±0.17)
air/3 h	13.15 (±0.18)	0.85 (±0.00)	63 (±0.5)	7.0 (±0.10)

DOI: 10.1021/am5087566
ACS Appl. Mater. Interfaces 2015, 7, 4826−4832

increase in R_s from 6 ± 3 to 9 ± 3 Ω cm^2 was observed when devices were processed in air. Even though this increase is small, it is sufficient to explain the observed subtle changes in EQE and TAE with air processing without having an obvious impact on other device parameters such as the FF.

Although the devices used to measure the TAE were encapsulated and the LiF/Al contact was never directly exposed to air, we believe that this small change in TAE is because of the LiF deposition directly on top of the air-exposed active layer. It has been shown that exposure of LiF to air ambient leads to chemical changes in the interlayer.[29] Based on a study from Glowacki et al., Al atoms deposited on top of LiF can cause LiF ions to diffuse into the underlying organic layer.[30] In the case of the Air devices, where the active layer was exposed to and may retain a small amount of residual oxygen and water, the reaction with LiF ions could cause a slight change in the total absorption of the device. This slight change was reflected in the TAE spectra. It should also be noted that the change in TAE is unlikely to have originated from degradation of PEDOT:PSS since, for both the Air device and the N_2 device, the PEDOT:PSS was directly exposed to air for the same period of time.

In order to verify the accuracy of our data and ensure that the absorption efficiency is actually lower for the Air devices, the EQEs were measured at 500 and 683 nm as a function of reverse bias. The wavelengths chosen for these measurements correspond to the regime where the EQEs are the same for both devices (λ = 683 nm) and the regime where there is a small difference in EQE (λ = 500 nm). The EQE dependence on the reverse bias for two specific wavelengths shown in Figure 2b was in good agreement with the TAE data. As anticipated, the data for the EQE as a function of voltage at 683 nm overlap and saturate at the same value under reverse bias. In the saturation region where the EQE value levels out, the charge collection efficiency is assumed to be 100% since all charge carriers are collected at the respective electrodes.[31] In contrast, at 500 nm, the two EQE curves are separated even at a large reverse bias, indicating that the absorption efficiency at 500 nm is indeed lower for the device made in air.

To further evaluate whether the difference in EQE is solely due to the difference in the device absorption, the internal quantum efficiencies (IQEs) for the two devices were determined using the EQE data and the TAE data for both devices.[32] The normalized IQE spectra for the two devices are shown in Figure 2c. The IQE spectrum for the N_2 device is almost flat at all wavelengths, and the IQE for the Air device is indeed lower at wavelengths below 550 nm. Since IQE only reflects the electrical properties in the device and does not take into account any difference in the total device absorption, this reduction in IQE at short wavelengths is solely due to electrical effects. The reduction in IQE at short wavelengths for the Air device confirms that the overall reduction in EQE is not only due to a reduction in the TAE but also due to other electrical effects.

In order to verify whether the changes in IQE come from electrical effects associated with charge transport, the electron and hole mobilities were measured using single carrier devices assuming the space−charge limited current (SCLC) model.[33] A detailed description of this method can be found in the literature.[34] As expected, the measured average electron mobilities for both devices are similar, i.e., (5 ± 0.2) × 10^{-4} cm^2/(V s) for the N_2 device and (2 ± 0.35) × 10^{-4} cm^2/(V s) for the Air device. This is in good agreement with what has recently been reported by Nicolai et al. on photo-oxidation defects as the products formed in the presence of water and oxygen in organic semiconductors.[35] Their findings suggest that for stable trap-free materials the target electron affinity of organic molecules should be larger than 3.6 eV. These numbers are consistent with multiple reports showing that organic molecules with electron affinities close to 4 eV or larger are less susceptible to reduction due to the presence of water and thus exhibit a higher level of air stability.[36,37] Since the electron affinity for $PC_{71}BM$ is around 4.3 eV, no change in charge transport was expected for electrons. One the other hand, the average hole mobilities for the N_2 device ((1.6 ± 0.3) × 10^{-4} cm^2/(V s)) are almost 1 order of magnitude larger than that for the Air device ((3 ± 0.7) × 10^{-5} cm^2/(V s)).

To determine whether the difference in hole mobilities is due to morphology, tapping-mode atomic force microscopy (AFM) measurements were performed on both active layers. Details about this technique can be found elsewhere.[38] Figures 3a and 3b show 5 μm × 5 μm topographic images of p(DTG-TPD):$PC_{71}BM$ films for the N_2 and Air devices. After air exposure there were no observable changes in the domain size and morphology. Even though AFM only probes the surface morphology, it is clear that the effect of air processing on the morphology of the films is very small. Even though subtle changes in morphology such as differences in intermixing on the molecular scale could be responsible for a small change in device performance, we believe it is more likely that the difference in hole mobilities is due to a higher trap density in the active layer upon air exposure as previously reported.[27]

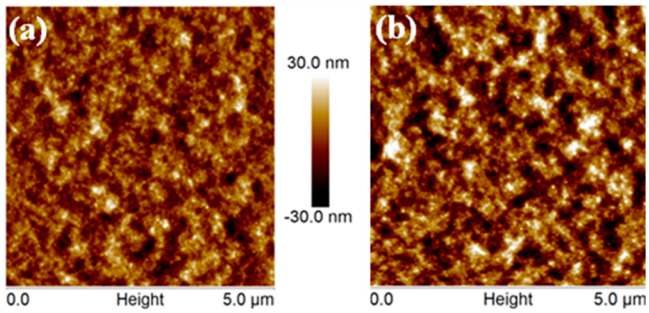

Figure 3. (a) 5 μm × 5 μm AFM topographic images of p(DTG-TPD):$PC_{71}BM$ films: (a) processed in nitrogen; (b) processed in air.

In order to gain a deeper understanding of the effect of hole transport on EQE, transfer matrix formalism (TMF) simulations were used to calculate the field distribution inside the device.[39,40] The optical modeling was based on the following stack of materials: ITO(90 nm)/PEDOT:PSS(30 nm)/p(DTG-TPD):$PC_{71}BM$(90 nm)/LiF(1 nm)/Al(100 nm). The optical model assumes that all surfaces are planar and all layers are isotropic.[41] The complex refractive indices for all materials were acquired using variable angle spectroscopic ellipsometry (VASE).[42] To acquire the electric field distribution inside the device, a constant energy radiator is applied to the optical model. The normalized electric field distribution can be seen in Figure 4a. The normalized optical electric field intensity in the device, $|E|^2$, corresponds to the absorption in the active layer and indicates that the distribution of the electric field inside the device is wavelength-dependent. The figure shows that there are two electric field intensity maxima within the active layer. The first maximum is located at short wavelengths

DOI: 10.1021/am5087566
ACS Appl. Mater. Interfaces 2015, 7, 4826−4832

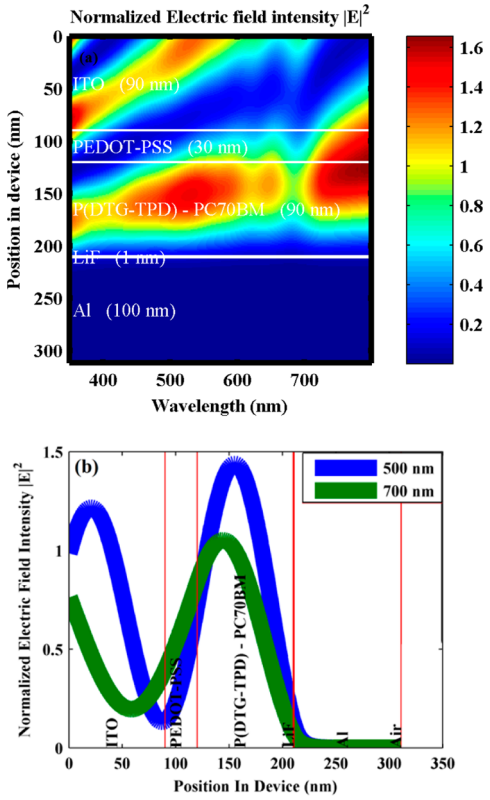

Figure 4. (a) Simulation for the normalized electric field intensity profile $|E|^2$ for the studied ITO/PEDOT:PSS/p(DTG-TPD):$PC_{71}BM$/LiF/Al structure. (b) Simulated optical field distribution for 500 and 700 nm illumination.

(450−600 nm), where the IQE spectra for the devices are different. This maximum is located closer to the center of the active layer, further away from the anode compared to the longer wavelength maximum (650−750 nm) which is located closer to the anode as shown in Figure 4a. For clarity, Figure 4b shows the electric field distribution inside the device for the two wavelengths of interest (500 and 700 nm).

Even though the positional shift in the peak electric field intensity is not large, i.e., ∼12 nm, a difference of a few nanometers is large enough to cause a change in device performance due to the low-mobility organic semiconductors.[43] This observation, in combination with the degraded hole mobilities, suggests that the difference in photocurrent between the two devices is due to the change in the number of holes reaching the electrodes.[44] Since holes from photons with wavelengths between 400 and 600 nm are generated farther away from the anode and have lower mobilities in the Air devices, they are less likely to be extracted, leading to a reduction in photocurrent. Hence, lower hole mobilities due to air exposure account for most of the decrease in the EQE in the short-wavelength region resulting in a reduction in J_{sc}. It is worth highlighting that the reduction in J_{sc} is less than 10% and part of it is also due to a small decrease in TAE as mentioned above.

The data above show the effects of air exposure for 10 min on device performance. While this exposure time is sufficient for processing in laboratory environments, a longer air exposure might be required in manufacturing environments. In order to study the effect of prolonged air exposure, devices were fabricated from films intentionally exposed to air for up to 3 h. Figure 5a shows the $J-V$ characteristics for devices fabricated in air and kept in ambient conditions for 1, 2, and 3 h, compared

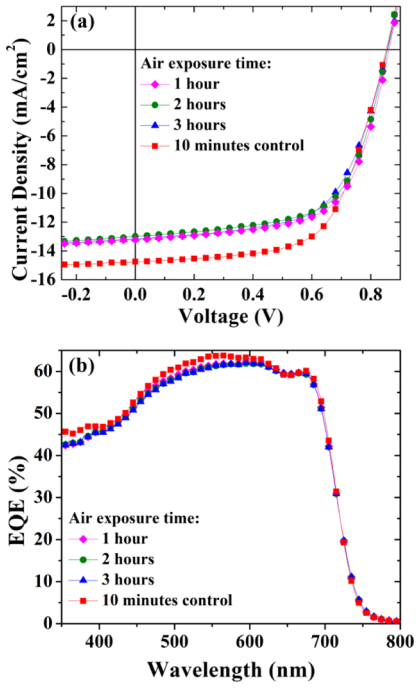

Figure 5. (a) $J-V$ curves of the solar cells made in air for different air exposure times. (b) EQE spectra for devices made in air for different air exposure times.

to a device made in air and kept in air for 10 min. Once again, the device parameter most affected by the long air exposure is J_{sc}. A 10% decrease in current was observed as the air exposure time increases from 10 min to 1 h, whereas no changes in FF or V_{oc} were observed. Surprisingly, almost no further degradation was observed for devices kept in air for two additional hours. A summary of the average device parameters is given in Table 1. Further, the EQE data for these devices depicted in Figure 5b showed the same trend as before where the device degradation was only obvious in EQE at shorter wavelengths. Based on the air exposure time data, it is reasonable to assume that most of the degradation in the active layer is due to the first hour of air exposure.

4. SUMMARY AND CONCLUSIONS

In conclusion, we have presented high-efficiency, air-stable p(DTG-TPD):$PC_{71}BM$ PSCs processed in air with PCEs up to 7.7% compared to 8.5% for devices processed in nitrogen. It was found that upon exposure to air, devices exhibited a lower J_{sc} than devices processed in nitrogen, while V_{oc} and FF were mostly unaffected. Optical and electrical characterization, as well as optical simulations, indicate that the reduction in photocurrent originates partly from a decrease in the TAE of the device due to changes in the cathode, while the remaining decrease is attributed to a decrease in hole mobility. Finally, our data show that with a high level of air stability and power conversion efficiency, p(DTG-TPD):$PC_{71}BM$ is a promising candidate for roll-to-roll processing.

AUTHOR INFORMATION

Corresponding Author

*E-mail: fso@mse.ufl.edu.

DOI: 10.1021/am5087566
ACS Appl. Mater. Interfaces 2015, 7, 4826−4832

Present Address
[§]Dewei Zhao, Department of Physics and Astronomy: University of Toledo, Toledo, OH 43606.

Author Contributions
The manuscript was written through contributions of all authors. All authors have given approval to the final version of the manuscript.

Notes
The authors declare no competing financial interest.

■ ACKNOWLEDGMENTS

The authors acknowledge the support of the Office of Naval Research (Award N000141110245), and F.S. acknowledges the support of the Florida Energy Systems Consortium (FESC). The authors also acknowledge Dr. Yuan Li for providing the software used in this study.

■ REFERENCES

(1) Darling, S. B.; You, F. The Case for Organic Photovoltaics. *RSC Adv.* **2013**, *3*, 17633−17648.
(2) Kaltenbrunner, M.; White, M. S.; Głowacki, E. D.; Sekitani, T.; Someya, T.; Sariciftci, N. S.; Bauer, S. Ultrathin and Lightweight Organic Solar Cells with High Flexibility. *Nat. Commun.* **2012**, *3*, 770.
(3) Liao, S.-H.; Jhuo, H.-J.; Cheng, Y.-S.; Chen, S.-A. Fullerene Derivative-Doped Zinc Oxide Nanofilm as the Cathode of Inverted Polymer Solar Cells with Low-Bandgap Polymer (PTB7-Th) for High Performance. *Adv. Mater.* **2013**, *25*, 4766−4771.
(4) Chen, J.-D.; Cui, C.; Li, Y.-Q.; Zhou, L.; Ou, Q.-D.; Li, C.; Li, Y.; Tang, J.-X. Single-Junction Polymer Solar Cells Exceeding 10% Power Conversion Efficiency. *Adv. Mater.* **2015**, *27*, 1035−1041.
(5) Kan, B.; Zhang, Q.; Li, M.; Wan, X.; Ni, W.; Long, G.; Wang, Y.; Yang, X.; Feng, H.; Chen, Y. Solution-Processed Organic Solar Cells Based on Dialkylthiol-Substituted Benzodithiophene Unit with Efficiency Near 10%. *J. Am. Chem. Soc.* **2014**, *136*, 15529−15532.
(6) Facchetti, A. Polymer Donor−Polymer Acceptor (All-Polymer) Solar Cells. *Mater. Today* **2013**, *16*, 123−132.
(7) Krebs, F. C.; Gevorgyan, S. A.; Alstrup, J. A Roll-to-Roll Process to Flexible Polymer Solar Cells: Model Studies, Manufacture and Operational Stability Studies. *J. Mater. Chem.* **2009**, *19*, 5442−5451.
(8) Søndergaard, R. R.; Hösel, M.; Krebs, F. C. Roll-to-Roll Fabrication of Large Area Functional Organic Materials. *J. Polym. Sci., Part B: Polym. Phys.* **2013**, *51*, 16−34.
(9) Krebs, F. C. Fabrication and Processing of Polymer Solar Cells: A Review of Printing and Coating Techniques. *Sol. Energy Mater. Sol. Cells* **2009**, *93*, 394−412.
(10) Søndergaard, R.; Hösel, M.; Angmo, D.; Larsen-Olsen, T. T.; Krebs, F. C. Roll-to-Roll Fabrication of Polymer Solar Cells. *Mater. Today* **2012**, *15*, 36−49.
(11) You, J.; Dou, L.; Yoshimura, K.; Kato, T.; Ohya, K.; Moriarty, T.; Emery, K.; Chen, C.-C.; Gao, J.; Li, G.; Yang, Y. A Polymer Tandem Solar Cell with 10.6% Power Conversion Efficiency. *Nat. Commun.* **2013**, *4*, 1446.
(12) Betancur, R.; Maymó, M.; Elias, X.; Vuong, L. T.; Martorell, J. Sputtered NiO as Electron Blocking Layer in P3HT:PCBM Solar Cells Fabricated in Ambient Air. *Sol. Energy Mater. Sol. Cells* **2011**, *95*, 735−739.
(13) Bovill, E. S. R.; Griffin, J.; Wang, T.; Kingsley, J. W.; Yi, H.; Iraqi, A.; Buckley, A. R.; Lidzey, D. G. Air Processed Organic Photovoltaic Devices Incorporating a MoOx Anode Buffer Layer. *Appl. Phys. Lett.* **2013**, *102*, 183303.
(14) Wu, S.; Li, J.; Tai, Q.; Yan, F. Investigation of High-Performance Air-Processed Poly(3-hexylthiophene)/Methanofullerene Bulk-Heterojunction Solar Cells. *J. Phys. Chem. C* **2010**, *114*, 21873−21877.
(15) Wu, Q.; Bhattacharya, M.; Moore, L. M. J.; Morgan, S. E. Air Processed P3HT:PCBM Photovoltaic Cells: Morphology Correlation to Annealing, Degradation, and Recovery. *J. Polym. Sci., Part B: Polym. Phys.* **2014**, *52*, 1511−1520.
(16) Abdou, M. S. A.; Orfino, F. P.; Xie, Z. W.; Deen, M. J.; Holdcroft, S. Reversible Charge Transfer Complexes Between Molecular Oxygen and Poly(3-alkylthiophene)s. *Adv. Mater.* **1994**, *6*, 838−841.
(17) Bellani, S.; Fazzi, D.; Bruno, P.; Giussani, E.; Canesi, E. V.; Lanzani, G.; Antognazza, M. R. Reversible P3HT/Oxygen Charge Transfer Complex Identification in Thin Films Exposed to Direct Contact with Water. *J. Phys. Chem. C* **2014**, *118*, 6291−6299.
(18) Angmo, D.; Gevorgyan, S. A.; Larsen-Olsen, T. T.; Søndergaard, R. R.; Hösel, M.; Jørgensen, M.; Gupta, R.; Kulkarni, G. U.; Krebs, F. C. Scalability and Stability of Very Thin, Roll-to-Roll Processed, Large Area, Indium-Tin-Oxide Free Polymer Solar Cell Modules. *Org. Electron.* **2013**, *14*, 984−994.
(19) Kakavelakis, G.; Stratakis, E.; Kymakis, E. Synergetic Plasmonic Effect of Al and Au Nanoparticles for Efficiency Enhancement of Air Processed Organic Photovoltaic Devices. *Chem. Commun.* **2014**, *50*, 5285−5287.
(20) Mateker, W. R.; Douglas, J. D.; Cabanetos, C.; Sachs-Quintana, I. T.; Bartelt, J. A.; Hoke, E. T.; El Labban, A.; Beaujuge, P. M.; Frechet, J. M. J.; McGehee, M. D. Improving the Long-Term Stability of PBDTTPD Polymer Solar Cells through Material Purification Aimed at Removing Organic Impurities. *Energy Environ. Sci.* **2013**, *6*, 2529−2537.
(21) Alem, S.; Wakim, S.; Lu, J.; Robertson, G.; Ding, J.; Tao, Y. Degradation Mechanism of Benzodithiophene-Based Conjugated Polymers When Exposed to Light in Air. *ACS Appl. Mater. Interfaces* **2012**, *4*, 2993−2998.
(22) Razzell-Hollis, J.; Wade, J.; Tsoi, W. C.; Soon, Y.; Durrant, J.; Kim, J.-S. Photochemical Stability of High Efficiency PTB7:PC70BM Solar Cell Blends. *J. Mater. Chem. A* **2014**, *2*, 20189−20195.
(23) Soon, Y. W.; Cho, H.; Low, J.; Bronstein, H.; McCulloch, I.; Durrant, J. R. Correlating Triplet Yield, Singlet Oxygen Generation and Photochemical Stability in Polymer/Fullerene Blend Films. *Chem. Commun.* **2013**, *49*, 1291−1293.
(24) Small, C. E.; Chen, S.; Subbiah, J.; Amb, C. M.; Tsang, S.-W.; Lai, T.-H.; Reynolds, J. R.; So, F. High-Efficiency Inverted Dithienogermole−Thienopyrrolodione-Based Polymer Solar Cells. *Nat. Photon.* **2012**, *6*, 115−120.
(25) Small, C. E.; Tsang, S.-W.; Chen, S.; Baek, S.; Amb, C. M.; Subbiah, J.; Reynolds, J. R.; So, F. Loss Mechanisms in Thick-Film Low-Bandgap Polymer Solar Cells. *Adv. Energy Mater.* **2013**, *3*, 909−916.
(26) Amb, C. M.; Chen, S.; Graham, K. R.; Subbiah, J.; Small, C. E.; So, F.; Reynolds, J. R. Dithienogermole as a Fused Electron Donor in Bulk Heterojunction Solar Cells. *J. Am. Chem. Soc.* **2011**, *133*, 10062−10065.
(27) Nam, C.-Y.; Su, D.; Black, C. T. High-Performance Air-Processed Polymer−Fullerene Bulk Heterojunction Solar Cells. *Adv. Funct. Mater.* **2009**, *19*, 3552−3559.
(28) Hoppe, H.; Arnold, N.; Sariciftci, N. S.; Meissner, D. Modeling the Optical Absorption within Conjugated Polymer/Fullerene-Based Bulk-Heterojunction Organic Solar Cells. *Sol. Energy Mater. Sol. Cells* **2003**, *80*, 105−113.
(29) Yang, L.; Xu, H.; Tian, H.; Yin, S.; Zhang, F. Effect of Cathode Buffer Layer on the Stability of Polymer Bulk Heterojunction Solar Cells. *Sol. Energy Mater. Sol. Cells* **2010**, *94*, 1831−1834.
(30) Głowacki, E. D.; Marshall, K. L.; Tang, C. W.; Sariciftci, N. S. Doping of Organic Semiconductors Induced by Lithium Fluoride/Aluminum Electrodes Studied by Electron Spin Resonance and Infrared Reflection-Absorption Spectroscopy. *Appl. Phys. Lett.* **2011**, *99*, 043305.
(31) Pandey, R.; Holmes, R. J. Characterizing the Charge Collection Efficiency in Bulk Heterojunction Organic Photovoltaic Cells. *Appl. Phys. Lett.* **2012**, *100*, 083303.
(32) Park, S. H.; Roy, A.; Beaupre, S.; Cho, S.; Coates, N.; Moon, J. S.; Moses, D.; Leclerc, M.; Lee, K.; Heeger, A. J. Bulk Heterojunction Solar Cells with Internal Quantum Efficiency Approaching 100%. *Nat. Photon.* **2009**, *3*, 297−302.

DOI: 10.1021/am5087566
ACS Appl. Mater. Interfaces 2015, 7, 4826−4832

(33) Chen, S.; Choudhury, K. R.; Subbiah, J.; Amb, C. M.; Reynolds, J. R.; So, F. Photo-Carrier Recombination in Polymer Solar Cells Based on P3HT and Silole-Based Copolymer. *Adv. Energy Mater.* **2011**, *1*, 963−969.
(34) Mihailetchi, V. D.; Wildeman, J.; Blom, P. W. M. Space-Charge Limited Photocurrent. *Phys. Rev. Lett.* **2005**, *94*, 126602.
(35) Nicolai, H. T.; Kuik, M.; Wetzelaer, G. A. H.; de Boer, B.; Campbell, C.; Risko, C.; Brédas, J. L.; Blom, P. W. M. Unification of Trap-Limited Electron Transport in Semiconducting Polymers. *Nat. Mater.* **2012**, *11*, 882−887.
(36) Anthopoulos, T. D.; Anyfantis, G. C.; Papavassiliou, G. C.; de Leeuw, D. M. Air-Stable Ambipolar Organic Transistors. *Appl. Phys. Lett.* **2007**, *90*, 122105.
(37) Zhuo, J.-M.; Zhao, L.-H.; Png, R.-Q.; Wong, L.-Y.; Chia, P.-J.; Tang, J.-C.; Sivaramakrishnan, S.; Zhou, M.; Ou, E. C. W.; Chua, S.-J.; Sim, W.-S.; Chua, L.-L.; Ho, P. K. H. Direct Spectroscopic Evidence for a Photodoping Mechanism in Polythiophene and Poly-(bithiophene-*alt*-thienothiophene) Organic Semiconductor Thin Films Involving Oxygen and Sorbed Moisture. *Adv. Mater.* **2009**, *21*, 4747−4752.
(38) Chen, W.; Nikiforov, M. P.; Darling, S. B. Morphology Characterization in Organic and Hybrid Solar Cells. *Energy Environ. Sci.* **2012**, *5*, 8045−8074.
(39) Chen, K.-S.; Salinas, J.-F.; Yip, H.-L.; Huo, L.; Hou, J.; Jen, A. K. Y. Semi-Transparent Polymer Solar Cells with 6% PCE, 25% Average Visible Transmittance and a Color Rendering Index Close to 100 for Power Generating Window Applications. *Energy Environ. Sci.* **2012**, *5*, 9551−9557.
(40) Hoppe, H.; Arnold, N.; Meissner, D.; Sariciftci, N. S. Modeling of Optical Absorption in Conjugated Polymer/Fullerene Bulk-Heterojunction Plastic Solar Cells. *Thin Solid Films* **2004**, *451−452*, 589−592.
(41) Pettersson, L. A. A.; Roman, L. S.; Inganäs, O. Modeling Photocurrent Action Spectra of Photovoltaic Devices Based on Organic Thin Films. *J. Appl. Phys.* **1999**, *86*, 487−496.
(42) Tammer, M.; Monkman, A. P. Measurement of the Anisotropic Refractive Indices of Spin Cast Thin Poly(2-methoxy-5-(2′-ethyl-hexyloxy)-*p*-phenylenevinylene) (MEH−PPV) Films. *Adv. Mater.* **2002**, *14*, 210−212.
(43) Myers, J. D.; Tseng, T.-K.; Xue, J. Photocarrier Behavior in Organic Heterojunction Photovoltaic Cells. *Org. Electron.* **2009**, *10*, 1182−1186.
(44) Dibb, G. F. A.; Muth, M.-A.; Kirchartz, T.; Engmann, S.; Hoppe, H.; Gobsch, G.; Thelakkat, M.; Blouin, N.; Tierney, S.; Carrasco-Orozco, M.; Durrant, J. R.; Nelson, J. Influence of Doping on Charge Carrier Collection in Normal and Inverted Geometry Polymer:-Fullerene Solar Cells. *Sci. Rep.* **2013**, *3*, 3335.

DOI: 10.1021/am5087566
ACS Appl. Mater. Interfaces 2015, 7, 4826−4832